Proceedings of DSCC 2008
ASME 2008 Dynamic Systems and Control Conference
October 20-22, 2008, Ann Arbor, Michigan, USA

DSCC2008-12345

DRAFT: A ROBUST APPROACH TO DYNAMIC FEEDBACK LINEARIZATION FOR A STEERABLE NIPS MECHANISM

Edgar I. Ergueta
Dept. of Mechanical Engineering
University of California
Berkeley, California 94720
Email: eergueta@me.berkeley.edu

Robert Seifried
Institute of Engineering
and Computational Mechanics
University of Stuttgart
70550 Stuttgart, Germany
Email: seifried@itm.uni-stuttgart.de

Roberto Horowitz
Dept. of Mechanical Engineering
University of California
Berkeley, California 94720
Email: horowitz@me.berkeley.edu

ABSTRACT

This paper presents two different control strategies for paper position control in printing devices. The first strategy is based on feedback linearization plus dynamic extension (dynamic feedback linearization). Even though this controller is very simple to design, we show that it is not able to handle multiplicative uncertainties, and therefore it fails when it is implemented on the experimental setup. The second strategy we present uses similar concepts, but it is more robust since feedback linearization is used only to linearize the kinematics of the system and internal loops are used to locally control the actuator's positions and velocities. Not only do we prove the robustness of the second control strategy, but we also show its successful implementation.

1 INTRODUCTION

Static feedback linearization is a nonlinear technique widely used for the control of MIMO nolinear systems. As explained in [1] and [2], it consists in differentiating each of the outputs several times until at least one of the inputs appears. At that point we obtain a decoupling matrix, which needs to be inverted in order to linearize the system. Once the system is linearized through this transformation, pole placement is used. Unfortunately, sometimes this decoupling matrix is singular, making static feedback linearization fail.

A common solution to this problem ([1], [2], [3], and [4]) consists on adding integrators to some of the input channels in order to delay the appearance of the inputs when differentiating the outputs. Proceeding in this way, it might be possible to construct a new decoupling matrix that can be inverted. This strategy is usually referred as dynamic feedback linearization. However, even if we succeed in finding an invertible decoupling matrix, the control strategy can be very sensible to model parameter uncertainties. For such cases, it is sometimes advised to modify this technique in order to gain in robustness.

In this paper we show how dynamic feedback linearization cannot be directly implemented in a mechatronic application for paper position control on printing devices. Specifically, this mechanism is located upstream from the image transfer station (ITS) and it has the objective to accurately position the page as it arrives to the ITS. As an alternative to the dynamic feedback linearization controller, a new control strategy is proposed, in which feedback linearization is used to linearize only the kinematics of the system, and internal loops are used to locally control the actuators's positions and velocities. This mechatronic application has been presented in [5] and [6]. The idea behind this mechanism is shown in Fig. 1 (US Patent Number 6,634,521) and it consists in two steerable nips that permits the control of the longitudinal, lateral, and angular positions of a sheet, while it is being driven forward. As mentioned in [5] and [6] this mechanism resembles that of a two-wheel robot [7]; however, whereas pavement cannot buckle in the two-wheel robot, sheets can in our system.

The remainder of this paper is organized as follows. Section 2 describes the steerable nips mechanism and presents its model. Section 3 presents the development of a dynamic feedback linearization controller for this application and shows how it fails when multiplicative uncertainties on the actuator plants are considered. Section 4 presents the robust control strategy implemented on the experimental setup and Section 5 proves its robustness. Moreover, experimental results for both controllers are shown in this section. Finally, some concluding remarks are stated in Section 6.

Copyright © 2008 by ASME

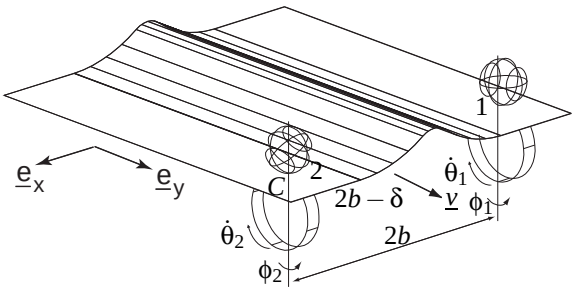

Figure 1. Steerable Nips with Paper Buckle

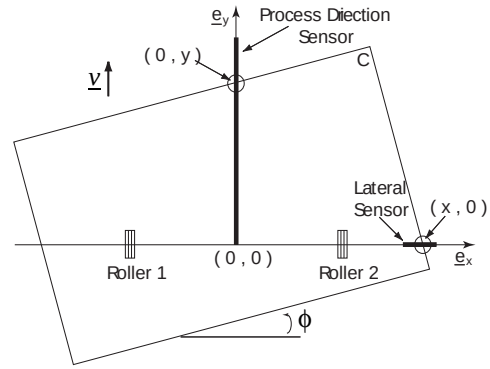

Figure 2. Top View of Steerable Nips

2 STEERABLE NIPS MECHANISM

Figure 1 shows a sheet while it is moving along a flat surface through the steerable nips mechanism. This mechanism has been designed so that it can correct for lateral sheet position errors without having to translate any actuators and without inflicting any damage on the paper. This is possible by steering the two rollers shown in the figure, which are underneath a backer ball. As a result, each roller is in contact with the sheet at only one point, letting the sheets safely move laterally while they are being driven forward. The roller is driven by a servo motor (*process direction motor*) attached to a rotating table, which is in turn steered by another servo motor (*steering motor*). A complete description of this mechanism can be found in [6].

In Fig. 1, the two rollers, located at points 1 and 2, are separated by a fixed distance $2b$. In [8] and [9] we used the leading right corner of the sheet, point C, as a reference for controlling the lateral and longitudinal position of the page. There, we were able to show asymptotic convergence of the system for a sheet of finite length. However, if we have a page of infinite length, a very small error in angular position would translate into huge errors for the lateral and longitudinal positions of point C. For this reason, since this paper intends to analyze the robustness of two different control strategies, we will now refer to the lateral position of the page, x, as the point along the lateral edge of the sheet that is in contact with a fixed lateral sensor. Similarly, we will define the longitudinal position of the sheet, y, as the point along the leading edge of the sheet that is in contact with a fixed longitudinal sensor; ϕ will represent the angular position of the sheet. These definitions can be better understood by looking at Fig. 2. Note that since the two rollers steer independently, the sheet can also buckle or stretch. Thus we need to keep buckling at a minimum and make sure that the sheet never stretches. As shown in Fig. 1, we define the amount of buckling of the sheet, δ, as the difference between the distance separating points 1 and 2 as measured along the paper $(2b-\delta)$ and along the straight line $(2b)$. Furthermore, $\dot{\theta}_i$ $(i=1,2)$ represent the angular velocity of the rollers in the direction parallel to the sheet, and ϕ_i $(i=1,2)$ represents their angular position in the direction perpendicular to the sheet.

The steerable nips mechanism has four nonholonomic constraints, which come from nonslip conditions on the rollers and local velocities (of the paper) being zero in the direction perpendicular to the rotation of the rollers. Thus, its kinematics model is derived so that these constraints are satisfied at all times; they are represented by the following equations:

$$
\begin{aligned}
\dot{x} &= r_1\dot{\theta}_1\left(\tfrac{x-b-\delta}{2b+\delta}\tan\phi\cos\phi_1+\sin\phi_1\right)\\
&\quad -r_2\dot{\theta}_2\left(\tfrac{x-b-\delta}{2b+\delta}\tan\phi\cos\phi_2\right) := f_x(\underline{x})\\
\dot{y} &= r_1\dot{\theta}_1\left(\tfrac{y\tan\phi-b-\delta}{2b+\delta}\cos\phi_1-\tan\phi\sin\phi_1\right)\\
&\quad -r_2\dot{\theta}_2\left(\tfrac{y\tan\phi-b-\delta}{2b+\delta}+1\right)\cos\phi_2 := f_y(\underline{x})\\
\dot{\phi} &= \tfrac{1}{2b+\delta}(r_1\cos\phi_1\dot{\theta}_1-r_2\cos\phi_2\dot{\theta}_2) := f_\phi(\underline{x})\\
\dot{\delta} &= r_2\sin\phi_2\dot{\theta}_2-r_1\sin\phi_1\dot{\theta}_1 := f_\delta(\underline{x})
\end{aligned}
\tag{1}
$$

where r_1 and r_2 are the radii of the two rollers and the state vector is given by $\underline{x}=[x\quad\phi\quad\delta\quad\phi_1\quad\phi_2\quad\dot{\theta}_2\quad\dot{\theta}_2\quad\dot{\phi}_1\quad\dot{\phi}_2]^T$. As expected from the definitions of x and y, Eq. (1) shows that x and y are completely decoupled. Finally, as mentioned in [6], a simple model that adequately described both the process direction and steering actuator dynamics is given by

$$
\begin{aligned}
\ddot{\theta}_i+\alpha_{pi}\dot{\theta}_i &= \beta_{pi}V_{pi};\quad (i=1,2)\\
\ddot{\phi}_i+\alpha_{si}\dot{\phi}_i &= \beta_{si}V_{si};\quad (i=1,2)
\end{aligned}
\tag{2}
$$

where V_{ji} is the voltage input to each motor, and α_{ji} and β_{ji} are coefficients that depend on the inertias and rotational viscous damping coefficients of the different components of the steerable nips mechanism. Subindexes p and s stand for process direction and steering actuators, respectively. Using Eqs. (1) and (2) we obtain the following state space representation:

$$
\frac{d}{dt}\begin{bmatrix} x\\ \phi\\ \delta\\ \phi_1\\ \phi_2\\ \dot{\theta}_1\\ \dot{\theta}_2\\ \dot{\phi}_1\\ \dot{\phi}_2 \end{bmatrix}
=
\begin{bmatrix} f_x(\underline{x})\\ f_\phi(\underline{x})\\ f_\delta(\underline{x})\\ \dot{\phi}_1\\ \dot{\phi}_2\\ -\alpha_{p1}\dot{\theta}_1\\ -\alpha_{p2}\dot{\theta}_2\\ -\alpha_{s1}\dot{\phi}_1\\ -\alpha_{s2}\dot{\phi}_2 \end{bmatrix}
+
\begin{bmatrix} 0&0&0&0\\ 0&0&0&0\\ 0&0&0&0\\ 0&0&0&0\\ 0&0&0&0\\ \beta_{p1}&0&0&0\\ 0&\beta_{p2}&0&0\\ 0&0&\beta_{s1}&0\\ 0&0&0&\beta_{s2} \end{bmatrix}
\begin{bmatrix} V_{p1}\\ V_{p2}\\ V_{s1}\\ V_{s2} \end{bmatrix}
\tag{3}
$$

$$
\underline{y}=\left[\,x\ \dot{y}_L\ \phi\ \delta\,\right]
$$

where $f_x(\underline{x})$, $f_\phi(\underline{x})$, and $f_\delta(\underline{x})$ are defined in Eqs. (1). Since this paper deals with the robust stability of the system, note that we

Copyright © 2008 by ASME

will now control the longitudinal velocity of the page at a fixed point L (the location of the image transfer station) instead of the longitudinal position, and thus $\dot{y}_L = f_y(\underline{x})$ evaluated at $y = L$.

3 DYNAMIC FEEDBACK LINEARIZATION CONTROLLER

As defined above, the control objective is to control the lateral and angular positions of the sheet before it arrives to the ITS as well as its velocity at that point. This needs to be accomplished within a finite pre-specified time and through the use of four control inputs. Two of these inputs rotate and steer one roller, and the other two inputs rotate and steer the other roller.

If we use static feedback linearization for this system, differentiating outputs x, ϕ, and δ twice, and output $\dot{y}_L$ once, we obtain an expression of the form

$$\left[\ddot{x}\ \ddot{y}_L\ \ddot{\phi}\ \ddot{\delta}\right]^T = A(\underline{x}) + B(\underline{x})\left[V_{p1}\ V_{p2}\ V_{s1}\ V_{s2}\right]^T \tag{4}$$

where the decoupling matrix $B(\underline{x})$ is singular. Thus, following the work presented in [1], [2], [3], and [4], in order to obtain a new nonsingular decoupling matrix, we need to add an integrator to the input channels corresponding to V_{p1} and V_{p2}. Proceeding in this way, V_{p1} and V_{p2} become new states of the system and their derivatives become two of the control inputs. Thus, we define the new states z_i ($i = 1,2$) and new control inputs w_i (i=1-4) as

$$\begin{aligned} z_1 = V_{p1};\ \ \dot{z}_1 = w_1 \\ z_2 = V_{p2};\ \ \dot{z}_2 = w_2 \\ w_3 = V_{s1} \\ w_4 = V_{s2} \end{aligned} \tag{5}$$

and obtain the following enlarged system:

$$\frac{d}{dt}\begin{bmatrix} x \\ \phi \\ \delta \\ \phi_1 \\ \phi_2 \\ \dot{\theta}_1 \\ \dot{\theta}_2 \\ \dot{\phi}_1 \\ \dot{\phi}_2 \\ z_1 \\ z_2 \end{bmatrix} = \begin{bmatrix} f_x(\underline{x}) \\ f_\phi(\underline{x}) \\ f_\delta(\underline{x}) \\ \dot{\phi}_1 \\ \dot{\phi}_2 \\ -\alpha_{p1}\dot{\theta}_{p1} + \beta_{p1}z_1 \\ -\alpha_{p2}\dot{\theta}_{p2} + \beta_{p2}z_2 \\ -\alpha_{s1}\dot{\phi}_{s1} \\ -\alpha_{s2}\dot{\phi}_{s2} \\ 0 \\ 0 \end{bmatrix} + \begin{bmatrix} 0 & 0 & 0 & 0 \\ 0 & 0 & 0 & 0 \\ 0 & 0 & 0 & 0 \\ 0 & 0 & 0 & 0 \\ 0 & 0 & 0 & 0 \\ 0 & 0 & 0 & 0 \\ 0 & 0 & 0 & 0 \\ 0 & 0 & \beta_{s1} & 0 \\ 0 & 0 & 0 & \beta_{s2} \\ 1 & 0 & 0 & 0 \\ 0 & 1 & 0 & 0 \end{bmatrix} \begin{bmatrix} w_1 \\ w_2 \\ w_3 \\ w_4 \end{bmatrix} \tag{6}$$

$$\underline{y} = \left[x\ \dot{y}_L\ \phi\ \delta\right]^T$$

where we can define the enlarged state vector as $\underline{x}_e = [x\ \ \phi\ \ \delta\ \ \phi_1\ \ \phi_2\ \ \dot{\theta}_2\ \ \dot{\phi}_1\ \ \dot{\phi}_2\ \ z_1\ \ z_2]^T$.

If we now differentiate outputs x, ϕ, and δ three times and output $\dot{y}_L$ twice, we obtain the expression

$$\left[\dddot{x}\ \dddot{y}_L\ \dddot{\phi}\ \dddot{\delta}\right]^T = A_e(\underline{x}_e) + B_e(\underline{x}_e)\left[w_1\ w_2\ w_3\ w_4\right]^T \tag{7}$$

where $A_e(\underline{x}_e)$ is a nonlinear vector and $B_e(\underline{x}_e)$ is a nonlinear square matrix. Since the inverse of matrix $B_e(\underline{x}_e)$ is

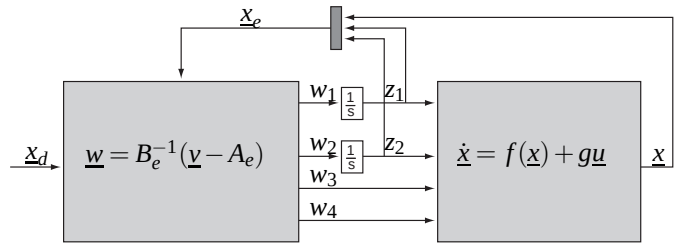

Figure 3. Dynamic Feedback Linearization Controller

$$B_e(\underline{x}_e)^{-1} = \begin{bmatrix} \frac{*}{\beta_{p1}r_1} & \frac{*}{\beta_{p1}r_1} & \frac{*}{\beta_{p1}r_1} & 0 \\ \frac{*}{\beta_{p2}r_2} & \frac{*}{\beta_{p2}r_2} & \frac{*}{2\beta_{p2}r_2} & \frac{*}{\beta_{p2}r_2} \\ \frac{*}{\beta_{s1}r_1\dot{\theta}_1} & \frac{*}{\beta_{s1}r_1\dot{\theta}_1} & \frac{*}{2\beta_{s1}r_1\dot{\theta}_1} & 0 \\ \frac{*}{\beta_{s2}r_2\dot{\theta}_2} & \frac{*}{\beta_{s2}r_2\dot{\theta}_2} & \frac{*}{2\beta_{s2}r_2\dot{\theta}_2} & \frac{*}{\beta_{s2}r_2\dot{\theta}_2} \end{bmatrix} \tag{8}$$

where $*'s$ are unspecified numerators that depend on the states, we notice that $B_e(\underline{x}_e)$ is invertible as long as the sheet is always moving in the process direction ($\dot{\theta}_1, \dot{\theta}_2 \neq 0$). Thus if we apply the feedback linearization control law

$$\begin{aligned} \left[w_1\ w_2\ w_3\ w_4\right]^T &= B_e(\underline{x}_e)^{-1}(\underline{v}(\underline{x}_e) - A_e(\underline{x}_e)) \\ \underline{v}(\underline{x}_e) &= \begin{bmatrix} \dddot{x}_d + k_x(\ddot{x}_d - \ddot{x}) + l_x(\dot{x}_d - \dot{x}) + \lambda_x(x_d - x) \\ \dddot{y}_d + k_y(\ddot{y}_d - \ddot{y}) + l_y(\dot{y}_d - \dot{y}) \\ \dddot{\phi}_d + k_\phi(\ddot{\phi}_d - \ddot{\phi}) + l_\phi(\dot{\phi}_d - \dot{\phi}) + \lambda_\phi(\phi_d - \phi) \\ \dddot{\delta}_d + k_\delta(\ddot{\delta}_d - \ddot{\delta}) + l_\delta(\dot{\delta}_d - \dot{\delta}) + \lambda_\delta(\delta_d - \delta) \end{bmatrix} \end{aligned} \tag{9}$$

by proper selection of gains $k's$, $l's$, and $\lambda's$ through pole placement, we can guarantee that the state errors converge to zero. Furthermore, since the enlarged system consist of 11 states and the relative degree is also 11, there are no internal dynamics, and we can conclude that the enlarged system is exponentially stable. The block diagram for this control strategy is shown in Fig. 3. Using this control law, for a sheet moving at a nominal velocity of $v = 0.5m/s$ and having initial errors $(x(0), \dot{y}_L(0), \phi(0), \delta(0)) = (8mm, 30mm/s, 2.5mrad, 0.1mm)$ we obtain the simulation results shown in Fig. 4. Even though Fig. 4 shows that the dynamic feedback linearization controller does a good job in reducing initial errors, it does not do that well when we introduce multiplicative uncertainty to each of the actuators as in Fig. 5. In this figure $P_{ji}(s)$ represents each of the actuator plants (Eqs. 2) and $\Delta_{ji}(s)$ represents the uncertainty dynamics. For this paper we assume these dynamics are given by

$$\Delta_{pi}(s) = \frac{\delta_{pi}}{(s+m_{pi})^2}; \quad \Delta_{si}(s) = \frac{\delta_{si}}{s+m_{si}}; \quad i = 1,2 \tag{10}$$

Figure 6 shows the results when multiplicative uncertainty is introduced to the system with $m_{pi} = m_{si} = 1.5$ and $\delta_{pi} = \delta_{si} = 1$ for $i = 1,2$. Here it is shown that the control strategy fails not

Copyright © 2008 by ASME

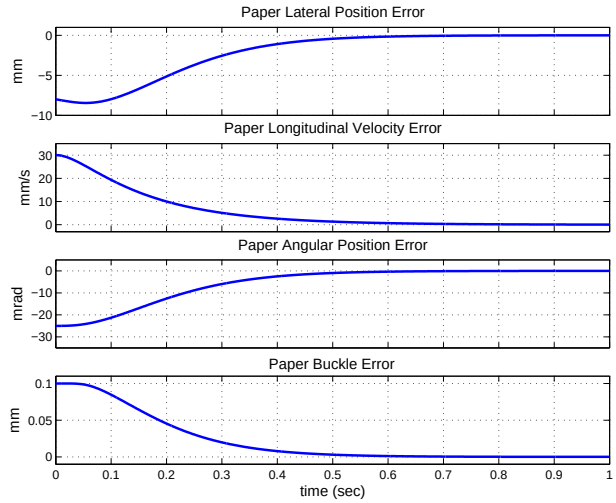

Figure 4. Simulation Results Using Dynamic Feedback Linearization Controller

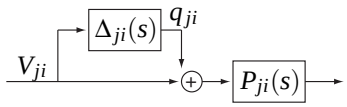

Figure 5. Multiplicative Uncertainty In Actuator Plants, where $j = s, p$ and $i = 1, 2$

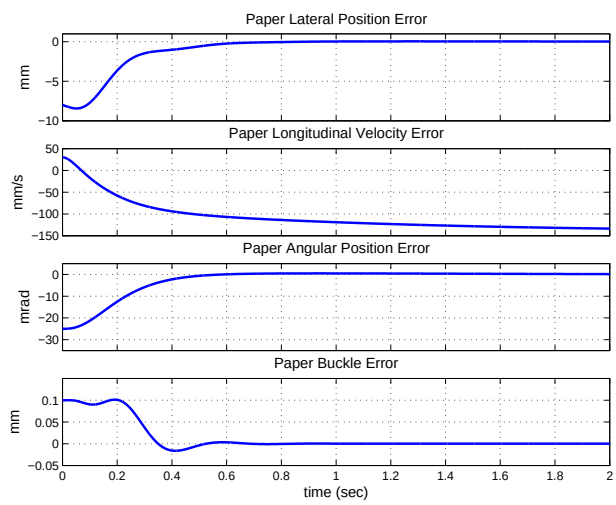

Figure 6. Simulation Results Using Dynamic Feedback Linearization Controller When Actuators Have Multiplicative Uncertainty

only because it is not able to eliminate errors in the longitudinal velocity of the sheet but also because it stretches the page (negative values for the error in buckling), which should never occur. Section 5 will compare the robustness of this control strategy to the one presented in the following section.

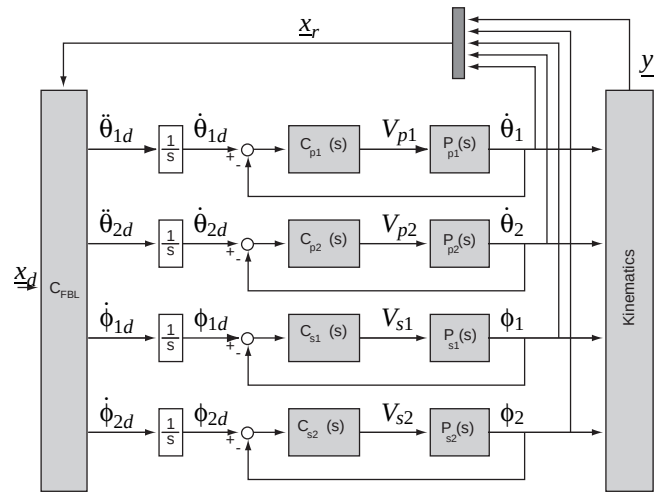

Figure 7. General Idea for Robust Dynamic Feedback Linearization Controller

4 ROBUST DYNAMIC FEEDBACK LINEARIZATION CONTROLLER

The control strategy presented in this section uses similar concepts to those described in Section 3, and its general idea is depicted in Fig. 7. As it can be seen in this figure, we first separate kinematics (Eqs. 1) from actuator dynamics (Eqs. (2)), which are represented by blocks P_{ji} (j=p,s; i=1,2), and then we linearize only the kinematics part of the system, considering the rotational velocities ($\dot{\theta}_1$ and $\dot{\theta}_2$) and steering positions (ϕ_1 and ϕ_2) of the rollers as inputs to the kinematics model. Then, a feedback linearization law, C_{FBL}, produces desired rotational accelerations and desired steering velocities, which after being integrated, are used as references to locally control the actuators.

Figure 8 shows the control strategy actually implemented to the real system. This controller uses the same idea as the one described in the previous paragraph, but it uses feedback plus feedforward to locally control the actuators. These local controllers are

$$\begin{aligned} C_{FB_{pi}}(s) &= \eta_{pi} + \frac{\gamma_{pi}}{s}; \quad C_{FF_{pi}} = \frac{1}{\beta_{pi}}(1 + \frac{\alpha_{pi}}{s}); \quad (i = 1,2) \\ C_{FB_{si}}(s) &= \eta_{si} + \gamma_{pi} s; \quad C_{FF_{pi}} = \frac{1}{\beta_{si}}(1 + \frac{\alpha_{si}}{s}); \quad (i = 1,2) \end{aligned} \tag{11}$$

where $\eta's$ and $\gamma's$ are controller gains. In order to be able to estimate the desired steering acceleration (needed for feedforward control), we use two first order filters, a technique called dynamic surface control and described in [10]. Note that if filter gain τ_i is sufficiently small, the value of $\dot{\phi}_{id}$ will be very close to that of $\dot{\tilde{\phi}}_i$ (for $i = 1,2$).

For the feedback linearization law, C_{FBL}, this time we need to differentiate outputs x, ϕ, and δ twice and output $\dot{y}_L$ once before the kinematics inputs appear, obtaining the following expression

$$\left[\ddot{x}\ \ddot{y}_L\ \ddot{\phi}\ \ddot{\delta}\right]^T = A_r(\underline{x}) + B_r(\underline{x})\left[\ddot{\theta}_1\ \ddot{\theta}_2\ \dot{\phi}_1\ \dot{\phi}_2\right]^T \tag{12}$$

Copyright © 2008 by ASME

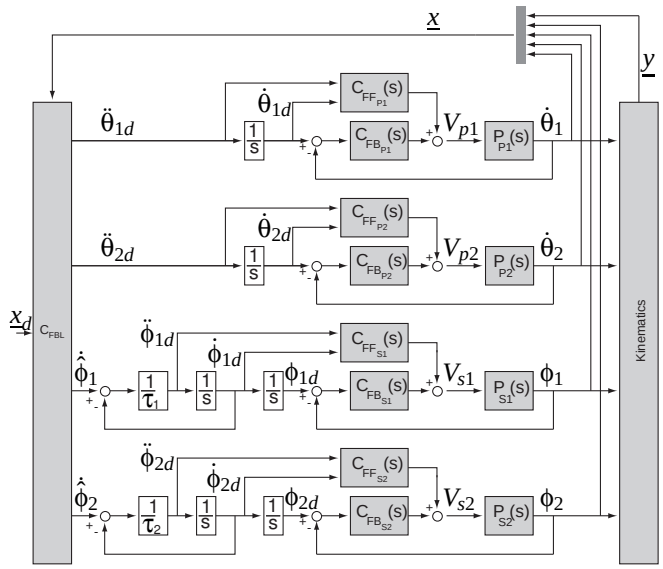

Figure 8. Robust Dynamic Feedback Linearization Controller Implemented

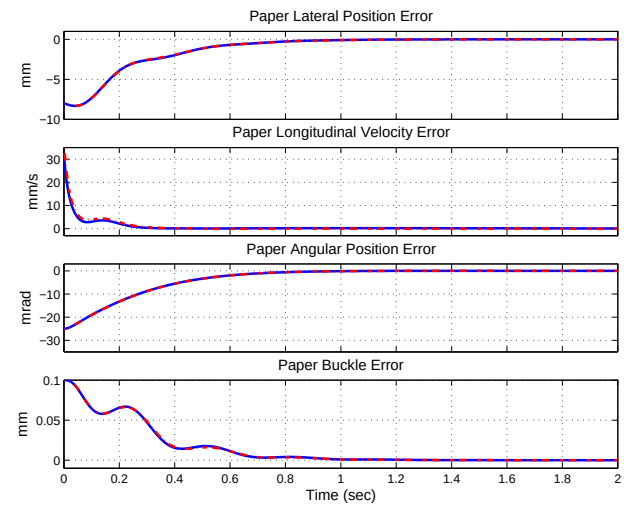

Figure 9. Simulation Results Using Robust Dynamic Feedback Linearization Controller. Note that the results without uncertainty (solid line) and those with uncertainty (dashed line) are almost indistinguishable.

where, again, $A_r(\underline{x})$ is a nonlinear vector, and $B_r(\underline{x})$ is a nonlinear square matrix. As in the previous section, since the inverse of matrix $B_r(\underline{x})$ is given by

$$B_r(\underline{x})^{-1} = \begin{bmatrix} \frac{*}{r_1(1+\tan^2\phi)} & \frac{*}{r_1(1+\tan^2\phi)} & \frac{*}{r_1(1+\tan^2\phi)} & 0 \\ \frac{*}{r_2(1+\tan^2\phi)} & \frac{*}{r_2(1+\tan^2\phi)} & \frac{*}{r_2(1+\tan^2\phi)} & \frac{*}{r_2} \\ \frac{*}{r_1\dot{\theta}_1(1+\tan^2\phi)} & \frac{*}{r_1\dot{\theta}_1(1+\tan^2\phi)} & \frac{*}{r_1\dot{\theta}_1(1+\tan^2\phi)} & 0 \\ \frac{*}{r_2\dot{\theta}_2(1+\tan^2\phi)} & \frac{*}{r_2\dot{\theta}_2(1+\tan^2\phi)} & \frac{*}{r_2\dot{\theta}_2(1+\tan^2\phi)} & \frac{*}{r_2\dot{\theta}_2} \end{bmatrix} \tag{13}$$

where $*'s$ are unspecified numerators that depend on the states, the decoupling matrix, $B_r(\underline{x})$, is invertible as long as the sheet is always moving along the process direction ($\dot{\theta}_1, \dot{\theta}_2 \neq 0$). Thus, we can apply the following feedback linearization law:

$$\begin{aligned} \left[\, \ddot{\theta}_{1d} \;\; \ddot{\theta}_{2d} \;\; \dot{\phi}_{1d} \;\; \dot{\phi}_{2d} \,\right]^T &= B_r(\underline{x})^{-1}(\underline{v}(\underline{x}) - A_r(\underline{x})) \\ \underline{v}(\underline{x}) &= \begin{bmatrix} \ddot{x}_d + (k_x+\lambda_x)(\dot{x}_d - \dot{x}) + k_x\lambda_x(x_d - x) \\ \ddot{y}_d + k_y(\dot{y}_d - \dot{y}) \\ \ddot{\phi}_d + (k_\phi+\lambda_\phi)(\dot{\phi}_d - \dot{\phi}) + k_\phi\lambda_\phi(\phi_d - \phi) \\ \ddot{\delta}_d + (k_\delta+\lambda_\delta)(\dot{\delta}_d - \dot{\delta}) + k_\delta\lambda_\delta(\delta_d - \delta) \end{bmatrix} \end{aligned} \tag{14}$$

where $k's$ and $\lambda's$ are the feedback linearization controller gains. Fig. 9 shows simulation results using the controller just presented. Note that in order to obtain these plots, we used the same initial conditions as those described in the previous section. Furthermore, this figure shows results for the cases with and without the uncertainties defined in Eqs. (10). As we can see in this figure, contrary to the results obtained using the controller described in Section 3, the robust dynamic feedback linearization controller presented in this section is able to correct for the initial errors of the sheet in both cases.

The stability of the closed-loop system can be shown by following exactly the same steps as those described in [8]. Furthermore, as explained in [8], we can also obtain a methodology to tune all the controller gains. In the next section, however, we will show the robustness of a slightly simplified version of the control strategy just presented.

5 ROBUSTNESS ANALYSIS

In this section we will first show exponential stability of the closed-loop system described in Section 4 and then we will compare its robustness to that of the dynamic feedback linearization controller presented in Section 3.

5.1 Stability Analysis of Robust Feedback Linearization Controller

For simplicity, let us first assume that the dynamics of the first order filters shown in Fig. 8 are very fast, so that we can estimate $\ddot{\phi}_d$ but we can set $\dot{\hat{\phi}}_i = \dot{\phi}_{id}$. Then, let us define paper coordinate errors and actuator errors by

$$\begin{aligned} \tilde{x} &= x_d - x; & \dot{\tilde{y}} &= \dot{y}_d - \dot{y}_L \\ \tilde{\phi} &= \phi_d - \phi; & \tilde{\delta} &= \delta_d - \delta \\ \varepsilon_{pi} &= \dot{\theta}_{id} - \dot{\theta}_i; & \varepsilon_{si} &= \phi_{id} - \phi_i; \;\; (i = 1,2) \end{aligned} \tag{15}$$

and let us also define the following surface errors:

$$\begin{aligned} s_x &= \dot{\tilde{x}} + \lambda_x\tilde{x}; & s_y &= \dot{\tilde{y}} \\ s_\phi &= \dot{\tilde{\phi}} + \lambda_\phi\tilde{\phi}; & s_\delta &= \dot{\tilde{\delta}} + \lambda_\phi\tilde{\delta} \\ s_{\varepsilon_{p1}} &= \dot{\varepsilon}_{p1} + \lambda_{\varepsilon_{p1}}\varepsilon_{p1}; & s_{\varepsilon_{p2}} &= \dot{\varepsilon}_{p2} + \lambda_{\varepsilon_{p2}}\varepsilon_{p2} \\ s_{\varepsilon_{s1}} &= \dot{\varepsilon}_{s1} + \lambda_{\varepsilon_{s1}}\varepsilon_{s1}; & s_{\varepsilon_{s2}} &= \dot{\varepsilon}_{s2} + \lambda_{\varepsilon_{s2}}\varepsilon_{s2} \end{aligned} \tag{16}$$

Combining Eqs. (12)-(15) we obtain the closed-loop expression

$$\left[\, \ddot{x} \;\; \dot{y}_L \;\; \ddot{\phi} \;\; \ddot{\delta} \,\right]^T = \underline{v}(\underline{x}) - A_r(\underline{x}) \left[\, \dot{\varepsilon}_{p1} \;\; \dot{\varepsilon}_{p2} \;\; \dot{\varepsilon}_{s1} \;\; \dot{\varepsilon}_{s2} \,\right]^T \tag{17}$$

Copyright © 2008 by ASME

If we further express $\underline{v}(\underline{x})$ in terms of paper and surface errors and let the gains γ_{pi} and η_{si} $(i=1,2)$ in Eqs. (11) be equal to:

$$\begin{aligned} \gamma_{pi} &= \frac{(\alpha_{pi}+\beta_{pi}\eta_{pi}-\lambda_{\varepsilon_{pi}})\lambda_{\varepsilon_{pi}}}{\beta_{pi}}; \quad (i=1,2) \\ \eta_{si} &= \frac{(\alpha_{si}+\gamma_{si}\beta_{si}-\lambda_{si})\lambda_{si}}{\beta_{si}}; \quad (i=1,2) \end{aligned} \tag{18}$$

the time derivatives of the errors above mentioned (Eqs. (15) and (16)) can be expressed as:

$$\begin{aligned} \dot{\tilde{x}} &= -\lambda_x\tilde{x}+s_x \\ \dot{\tilde{\phi}} &= -\lambda_\phi\tilde{\phi}+s_\phi \\ \dot{\tilde{\delta}} &= -\lambda_\delta\tilde{\delta}+s_\delta \\ \dot{\varepsilon}_{p1} &= -\lambda_{p1}\varepsilon_{p1}+s_{\varepsilon_{p1}} \\ \dot{\varepsilon}_{p2} &= -\lambda_{p2}\varepsilon_{p2}+s_{\varepsilon_{p2}} \\ \dot{\varepsilon}_{s1} &= -\lambda_{s1}\varepsilon_{s1}+s_{\varepsilon_{s1}} \\ \dot{\varepsilon}_{s2} &= -\lambda_{s2}\varepsilon_{s2}+s_{\varepsilon_{s2}} \\ \dot{s}_x &= -K_xs_x+b_{11}\dot{\varepsilon}_{p1}+b_{12}\dot{\varepsilon}_{p2}+b_{13}\dot{\varepsilon}_{s1}+b_{14}\dot{\varepsilon}_{s2} \\ \dot{s}_y &= -K_ys_y+b_{21}\dot{\varepsilon}_{p1}+b_{22}\dot{\varepsilon}_{p2}+b_{23}\dot{\varepsilon}_{s1}+b_{24}\dot{\varepsilon}_{s2} \\ \dot{s}_\phi &= -K_\phi s_\phi+b_{31}\dot{\varepsilon}_{p1}+b_{32}\dot{\varepsilon}_{p2}+b_{33}\dot{\varepsilon}_{s1}+b_{34}\dot{\varepsilon}_{s2} \\ \dot{s}_\delta &= -K_\delta s_\delta+b_{41}\dot{\varepsilon}_{p1}+b_{42}\dot{\varepsilon}_{p2}+b_{33}\dot{\varepsilon}_{s1}+b_{34}\dot{\varepsilon}_{s2} \\ \dot{s}_{\varepsilon_{p1}} &= -(\alpha_{p1}+\beta_{p1}\eta_{p1}-\lambda_{\varepsilon_{p1}})s_{\varepsilon_{p1}} \\ \dot{s}_{\varepsilon_{p2}} &= -(\alpha_{p2}+\beta_{p2}\eta_{p2}-\lambda_{\varepsilon_{p2}})s_{\varepsilon_{p2}} \\ \dot{s}_{\varepsilon_{s1}} &= -(\alpha_{s1}+\beta_{s1}\eta_{s1}-\lambda_{\varepsilon_{s1}})s_{\varepsilon_{s1}} \\ \dot{s}_{\varepsilon_{s2}} &= -(\alpha_{s2}+\beta_{s2}\eta_{s2}-\lambda_{\varepsilon_{s2}})s_{\varepsilon_{s2}} \end{aligned} \tag{19}$$

where b_{ij} is the (i,j) element of matrix $B_r(\underline{x})$. If we define the desired trajectory by $(x_d,\phi_d,\delta_d,\dot{x}_d,\dot{y}_d,\dot{\phi}_d,\dot{\delta}_d) = (0,0,0,0,\nu,0,0)$, where ν is the nominal longitudinal velocity of the sheet, and we linearize the system described in Eq. (19) around $\tilde{x}=\tilde{\phi}=\tilde{\delta}=\varepsilon_{p1}=\varepsilon_{p2}=\varepsilon_{s1}=\varepsilon_{s2}=s_x=s_y=s_\phi=s_\delta=s_{\varepsilon_{p1}}=s_{\varepsilon_{p2}}=s_{\varepsilon_{s1}}=s_{\varepsilon_{s2}}=0$, we can obtain an expression of the form

$$\dot{\underline{e}}(t) = G\underline{e}(t) \tag{20}$$

where $\underline{e}(t)$ is defined by

$$\underline{e}(t) = \left[\,\bar{x}\;\bar{y}\;\bar{\phi}\;\bar{\delta}\;\bar{\varepsilon}_{p1}\;\bar{\varepsilon}_{p2}\;\bar{\varepsilon}_{s1}\;\bar{\varepsilon}_{s2}\,\right]^T \tag{21}$$

$$\begin{aligned} &\bar{x}=\begin{bmatrix}\tilde{x}\\ s_x\end{bmatrix}; \qquad \bar{y}=s_y; \qquad \bar{\phi}=\begin{bmatrix}\tilde{\phi}\\ s_\phi\end{bmatrix}; \qquad \bar{\delta}=\begin{bmatrix}\tilde{\delta}\\ s_\delta\end{bmatrix} \\ &\bar{\varepsilon}_{p1}=\begin{bmatrix}\varepsilon_{p1}\\ s_{\varepsilon_{p1}}\end{bmatrix}; \bar{\varepsilon}_{p2}=\begin{bmatrix}\varepsilon_{p2}\\ s_{\varepsilon_{p2}}\end{bmatrix}; \bar{\varepsilon}_{s1}=\begin{bmatrix}\varepsilon_{s1}\\ s_{\varepsilon_{s1}}\end{bmatrix}; \bar{\varepsilon}_{s2}=\begin{bmatrix}\varepsilon_{s2}\\ s_{\varepsilon_{s2}}\end{bmatrix} \end{aligned} \tag{22}$$

and G is given by

$$G = \left[\begin{array}{cccc|cccc} A_x & 0 & 0 & 0 & 0 & 0 & B_x^{\varepsilon_{s1}} & 0 \\ 0 & A_y & 0 & 0 & B_y^{\varepsilon_{p1}} & B_y^{\varepsilon_{p2}} & 0 & 0 \\ 0 & 0 & A_\phi & 0 & B_\phi^{\varepsilon_{p1}} & B_\phi^{\varepsilon_{p2}} & 0 & 0 \\ 0 & 0 & 0 & A_\delta & 0 & 0 & B_\delta^{\varepsilon_{s1}} & B_\delta^{\varepsilon_{s2}} \\ \hline 0 & 0 & 0 & 0 & A_{\varepsilon_{p1}} & 0 & 0 & 0 \\ 0 & 0 & 0 & 0 & 0 & A_{\varepsilon_{p2}} & 0 & 0 \\ 0 & 0 & 0 & 0 & 0 & 0 & A_{\varepsilon_{s1}} & 0 \\ 0 & 0 & 0 & 0 & 0 & 0 & 0 & A_{\varepsilon_{s2}} \end{array}\right] \tag{23}$$

Note that the $A's$ in G depend only on controller gains and the $B's$ depend on controller gains as well as system parameters. Looking at Eq. (23), we can also express Eq. (20) as

$$\begin{bmatrix}\dot{n}_1\\ \dot{n}_2\end{bmatrix} = \left[\begin{array}{c|c} A_{n_1} & B_{n_1}^{n_2} \\ \hline 0 & A_{n_1} \end{array}\right]\begin{bmatrix} n_1\\ n_2\end{bmatrix} \tag{24}$$

and therefore, the solutions for $n_1(t)$ and $n_2(t)$ are given by

$$\begin{aligned} n_2(t) &= e^{A_{n_2}t}n_2(0) \\ n_1(t) &= e^{A_{n_1}t}n_1(0) + \left[\int_0^t e^{A_{n_1}(t-\tau)}B_{n_1}^{n_2}(\tau)e^{A_{n_2}\tau}d\tau\right]n_2(0) \end{aligned} \tag{25}$$

Then, it is easy to show that by proper selection of the controller gains, the linearized error dynamics are exponentially stable:

$$||\underline{e}(t)|| \le k||\underline{e}(0)||exp(-\gamma\, t) \tag{26}$$

Furthermore, if we define the Lyapunov function $v(\underline{e}) = \underline{e}^T P\underline{e}$, where P is the positive definite solution to the Lyapunov equation

$$G^TP + PA = -Q \tag{27}$$

and Q is any positive definite matrix, then we obtain the following bounds

$$\begin{aligned} \lambda_{min}(P)||\underline{e}||^2 \le v(\underline{e}) \le \lambda_{max}(P)||\underline{e}||^2 \\ \dot{v}(\underline{e}) \le -\lambda_{min}(Q)||\underline{e}||^2 \\ \left|\left|\frac{\partial v}{\partial \underline{e}}\right|\right| \le ||P||\;||\underline{e}|| \end{aligned} \tag{28}$$

5.2 Robustness of Both Controllers

Let us now analyze the robustness of the steerable nips mechanism when the robust dynamic feedback linearization controller presented in Section 4 is used. In order to do so, we will analyze its stability when we introduce the multiplicative uncertainty shown in Fig. 5 and Eqs. (10). Performing exactly the same steps as those performed section 5.1, the linearized error dynamics are given by

$$\dot{\underline{e}}(t) = G\underline{e}(t) - D\underline{q}(t) \tag{29}$$

where the error state vector $\underline{e}(t)$ and matrix G are given as before, the uncertainty state vector, $\underline{q}(t)$, is given by (see Fig. 5):

$$\underline{q}(t) = \left[\,q_{p1}\;q_{p2}\;q_{s1}\;q_{s2}\,\right]^T \tag{30}$$

and D is a constant matrix that depends only on β_{pi} and β_{si} $(i=1,2)$. Thus, we can put the system in the form of Fig. 10 where system H_1 is given by Eq. (29), H_2 includes the uncertainties of

Copyright © 2008 by ASME

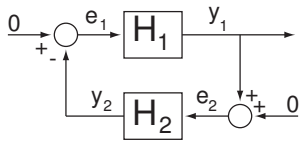

Figure 10. Feedback Connection for Small Gain Theorem

all four actuators (Eqs. (10)), $y_1 = [V_{p1}\ V_{p2}\ V_{s1}\ V_{s2}]^T$, and $y_2 = \underline{q}(t)$. If we can now show that both systems, H_1 and H_2, are finite gain L_∞ stable

$$\begin{array}{ll} (i)\ ||y_{1\tau}||_{L_\infty} \leq \gamma_1 ||e_{1\tau}||_{L_\infty} + \beta_1 & \forall e_1 \in L_\infty^4 \quad \forall \tau \in [0,\infty) \\ (ii)\ ||y_{2\tau}||_{L_\infty} \leq \gamma_2 ||e_{2\tau}||_{L_\infty} + \beta_2 & \forall e_2 \in L_\infty^4 \quad \forall \tau \in [0,\infty) \end{array} \tag{31}$$

with $\gamma_1\gamma_2 < 1$, then by the Small Gain Theorem ([2] and [11]) we can conclude that the feedback connection in Fig. 10 is also finite gain L_∞ stable. Note that in Eq. (31) we look at the truncation of functions up to time τ:

$$f_\tau = \begin{bmatrix} f(t), & 0, \leq t \leq \tau \\ 0, & \tau < t \end{bmatrix} \tag{32}$$

In order to show finite gain stability of systems H_1 and H_2 we need to use the following theorem, which is presented in [11]:

Theorem 5.1. *Consider the system*

$$\begin{array}{l} \dot{x} = f(t,x,u); \quad x(0) = x_o \\ y = h(t,x,u) \end{array} \tag{33}$$

Let $x \in I\!R^n$, $u \in I\!R^m$, $f : [0,\infty) x I\!R^n x I\!R^m \mapsto I\!R^n$ be piecewise continuous in t and Locally Lipschitz in (x,u), and $h : [0,\infty) x I\!R^n x I\!R^m \rightarrow I\!R^n$ be piecewise continuous in t and continuous in x,u. Further suppose that $x = 0$ is an exponentially stable equilibrium point of $\dot{x} = f(t,x,0)$ and there is a Lyapunov function that satisfies

$$\begin{array}{c} c_1||x||^2 \leq v(x) \leq c_2||x||^2 \\ \dot{v}(x) \leq -c_3||x||^2 \\ \left|\left|\frac{\partial v}{\partial x}\right|\right| \leq c_4||x|| \end{array} \tag{34}$$

for some positive constants c_1, c_2, c_3, c_4. Also f and h satisfy the inequalities

$$\begin{array}{c} ||f(t,x,u) - f(t,x,0)|| \leq L||u|| \\ ||h(t,x,u)|| \leq \eta_1||x|| + \eta_2||u|| \end{array} \tag{35}$$

for all $(t,x,u) \in [0,\infty) x I\!R^n x I\!R^m$ for some nonnegative constants L, η_1, and η_2. Then, system in Eq. (33) is finite gain L_∞ stable and the following inequality holds:

$$\begin{array}{c} ||y_\tau||_{L_\infty} \leq \gamma||u_\tau||_{L_\infty} + \beta, \quad \forall \tau \in [0,\infty) \\ \gamma = \eta_2 + \frac{\eta_1 c_2 c_4 L}{c_1 c_3}; \quad \beta = \eta_1||x_o||\sqrt{c_2/c_1} \end{array} \tag{36}$$

Robust Controller	Dynamic Controller
$\gamma_1 = 1.98$	$\gamma_1 = 1.87x10^{11}$
$\beta_1 = 0.41$	$\beta_1 = 1.20x10^3$
$\gamma_2 = 0.46$	$\gamma_2 = 0.45$
$\beta_2 = 0.002$	$\beta_2 = 0.003$

Table 1. Gains Required to Show bounds for Systems H_1 and H_2

The proof of this Theorem can be found in [11]. For our particular application, in Section 4 we showed that $\underline{e} = 0$ is an exponentially stable equilibrium point of Eq. (20), and constants $c_1 - c_4$ are given by Eq. (28). Furthermore, from Eq. (29) we have that $L = ||D||$. So, in order to compute gains γ_1 and β_1 in Eqs. (36) (required to satisfy the first condition in Eq. (31)), we only need to obtain gains η_1 and η_2 that satisfy the second condition in Eq. (35), where for our case $h(t,x,u) = y_1$ (see Fig. 10). We can similarly obtain gains γ_2 and β_2 to fulfill the second condition in Eq. (31). Then, by looking at Table 1 we have that $\gamma_1\gamma_2 < 1$, and therefore, from the Small Gain Theorem, we conclude that the closed-loop system is finite gain L_∞ stable when the multiplicative uncertainties defined in Eqs. (10) are used.

For the case of the dynamic feedback linearization controller described in Section 3, we can perform a similar analysis. First, we obtain the error dynamics

$$\dot{\underline{\tilde{x}}}_e = -f(\underline{\tilde{x}}_e) - D\underline{q}(t) \tag{37}$$

where $\underline{\tilde{x}}_e$ is the error state vector, $f(\underline{\tilde{x}}_e)$ is obtained by combining Eqs. (6), (9), and (10), and D and $\underline{q}(t)$ are defined exactly as before. After linearizing $f(\underline{\tilde{x}}_e)$ along $\underline{\tilde{x}}_e = 0$, we can put the system in the form of Fig. 10. We can then show exponential stability of $\underline{\tilde{x}}_e$ and obtain constants c_1-c_4 as in Eq. (28). After L, η_1, and η_2 are obtain as in the previous case, we use Eq. (36) to compute gains γ_1 and β_1. Gains γ_2 and β_2 are similarly obtained. This time, however, $\gamma_1\gamma_2 > 1$ (see Table 1), and thus we cannot conclude anything from the Small Gain Theorem, but such a large value for γ_1 indicates that the system may not be robust to multiplicative uncertainties in the actuators.

5.3 Experimental Results

The conclusions just made regarding the robustness of the two control strategies presented are justified not only by the simulation results shown in Figs. 6 and 9, but also through experimental tests. Figure 11 shows experimental results when a sheet of finite length was introduced to the steerable nips section and we used the robust dynamic feedback linearization controller described in Section 4. Here, the lateral and longitudinal position of the page is defined by the position of the leading right corner of the page (point C in Fig. 1). Figure 11 shows that we were able to correct the sheet's position in about 0.3 seconds. Note that the longitudinal position increases constantly because the sheet moves in the longitudinal direction at all times. The small

Copyright © 2008 by ASME

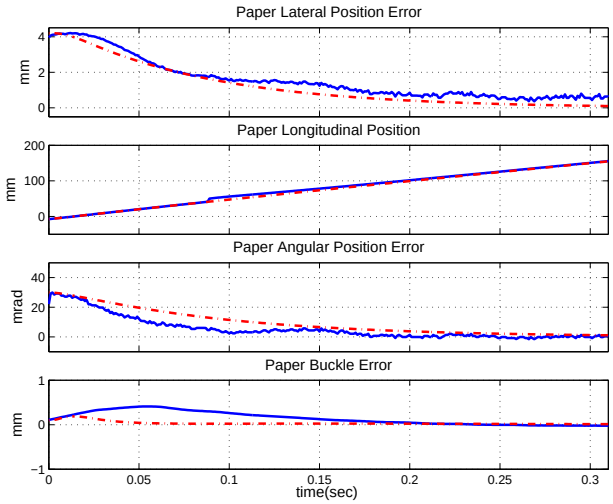

Figure 11. Experimental Results Using Robust Feedback Linearization Controller. The solid line is used for experimental results and the dashed line for simulation results.

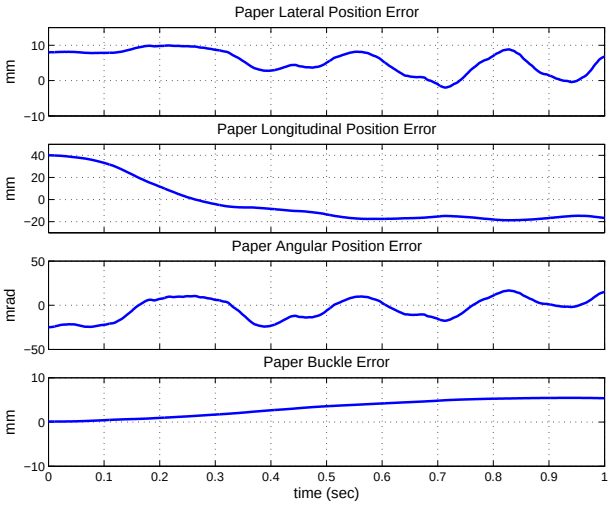

Figure 12. Experimental Results Using Dynamic Feedback Linearization Controller

discrepancies observed between simulation and experimental results can be attributed to sensor noise and un-modeled dynamics.

When the dynamic feedback linearization controller presented in Section 3 was tested on the experimental setup, it went unstable very quickly, and we were not able to collect any data since we did not want to risk the safety of our setup. However, in order to illustrate this instability, we performed a hybrid experiment, in which the real actuators were used, but we simulated the sheet by using the kinematic model. Those results are presented in Figure 12, which shows that this controller is not able to correct for the sheet initial position errors.

6 CONCLUSION

In this paper we have shown the drawbacks of using a controller simply based on dynamics feedback linearization due to un-modeled dynamics. Furthermore, we presented a robust modified version, which we call robust dynamic feedback linearization. Not only we proved that this control strategy is more robust to multiplicative uncertainties, but we also showed its successful implementation. This control strategy separates kinematics from actuator dynamics and uses feedback linearization only in the kinematics part of the system. Then we use internal loops to locally control the rotational velocity and steering position of the rollers through standard dynamic linear controllers.

ACKNOWLEDGMENT

This work was supported by the National Science Foundation under Grant CMS 0301719 and by financial support and collaboration from Xerox Corporation.

REFERENCES

[1] Isidori, A., 1995. *Nonlinear Control Systems*, 3rd ed. Springer.

[2] Sastry, S. S., 1999. *Nonlinear Systems : Analysis, Stability, and Control*. Springer.

[3] Descusse, J., and Moog, C., 1985. "Decoupling with dynamic compensation for strong invertible affine nonlinear systems". *Interantional Journal of Control*, **42**(6), pp. 1287–1398.

[4] d'Andrea Novel, B., Campion, G., and Bastin, G., 1995. "Control of noholonomic wheeled mobile robots by state feedback linearization". *The International Journal of Robotics Research*, **14**, pp. 543–559.

[5] Sanchez, R., Horowitz, R., and Tomizuka, M., 2004. "Paper sheet control using steerable nips". In 2004 American Control Conference Proceedings, pp. 482–487.

[6] Sanchez, R., Ergueta, E., Fine, B., Horowitz, R., Tomizuka, M., and Krucinskić, M., 2006. "A mechatronic approach to full sheet control using steer-able nips". In 4th IFAC Symposium in Mechatronic Systems.

[7] Yun, X., and Sarkar, N., 1996. "Dynamic feedback control of vehicles with two steerable wheels". In 1996 IEEE International Conference on Robotics and Automation, pp. 3105–3110.

[8] Ergueta, E., Sanchez, R., Horowitz, R., and Tomizuka, M., 2007. "Full sheet control through the use of steerable nips". In ASME International Mechanical Engineering Congress and Exposition.

[9] Ergueta, E., Sanchez, R., Horowitz, R., and Tomizuka, M., 2008. "Convergence analysis of a steerable nips mechanism for full sheet control in printing devices". *Submitted for publication at the Journal of Dynamics Systems, Measurement and Control*.

[10] Swaroop, D., Gerdes, J. C., Yip, P. P., and Hedrick, J. K., 1997. "Dynamic surface control of nonlinear systems". In Proceedings of the American Control Conference, pp. 3028 –3034.

[11] Khalil, H. K., 1996. *Nonlinear systems*, 2nd ed. Prentice Hall, Inc., N.J.

Copyright © 2008 by ASME